



Deposited via The University of Leeds.

White Rose Research Online URL for this paper:

<https://eprints.whiterose.ac.uk/id/eprint/141587/>

Version: Accepted Version

Article:

Nan, W and Ghadiri, M (2019) Numerical simulation of powder flow during spreading in additive manufacturing. *Powder Technology*, 342. pp. 801-807. ISSN: 0032-5910

<https://doi.org/10.1016/j.powtec.2018.10.056>

© 2018 Elsevier B.V. All rights reserved. Licensed under the Creative Commons Attribution-Non Commercial No Derivatives 4.0 International License (<https://creativecommons.org/licenses/by-nc-nd/4.0/>).

Reuse

This article is distributed under the terms of the Creative Commons Attribution-NonCommercial-NoDerivs (CC BY-NC-ND) licence. This licence only allows you to download this work and share it with others as long as you credit the authors, but you can't change the article in any way or use it commercially. More information and the full terms of the licence here: <https://creativecommons.org/licenses/>

Takedown

If you consider content in White Rose Research Online to be in breach of UK law, please notify us by emailing eprints@whiterose.ac.uk including the URL of the record and the reason for the withdrawal request.

Numerical Simulation of Powder Flow during Spreading in Additive Manufacturing

Wenguang Nan^{1,2}, Mojtaba Ghadiri^{2*}

1. School of Mechanical and Power Engineering, Nanjing Tech University, Nanjing 211816, China

2. School of Chemical and Process Engineering, University of Leeds, Leeds LS2 9JT, UK

*Contact Email: M.Ghadiri@leeds.ac.uk *Tel: 0044(0) 113 343 2406

Abstract: Additive manufacturing (AM) has attracted increasing attention in a wide range of applications, due to its ability for rapid manufacturing of complex shapes directly from a Computer-Aided Design (3D CAD) output. One of the manufacturing methods is based on powder processing, where a thin bed is formed to which an energy beam is applied to sinter and melt the powder. A major bottleneck in this method is associated with powder spreading, as its dynamics is sensitive to powder properties, machine design and operation conditions, such as speed of spreading. The effects of gap height and blade spreading speed on the evolving shear band and mass flow rate through the gap have been simulated by Discrete Element Method, using the most realistic physical and mechanical properties of the particles. It is shown that the particle velocity in the powder heap in front of the blade could well be described by a universal curve given by the Gauss error function. The mass flow rate through the gap increases linearly with the gap height. There exist two flow regimes with the increase of the blade spreading speed. Initially, the mass flow rate has a linear dependence on the blade speed, but eventually approaches an asymptotic value, implying a limit beyond which the mass flow rate cannot be further increased. This has an important implication on the speed of spreading.

Keywords: Additive Manufacturing; Particle Spreading; Sintering; Discrete Element Method; Shear band; Mass flow rate.

1 **1. Introduction**

2 Additive manufacturing (AM) is paving the way towards the next industrial revolution
3 [1-3]. AM creates three-dimensional (3D) objects by stepwise layer-by-layer approaches which
4 are controlled by a digital model. This unique feature allows the production of complex or
5 customized parts directly from the Computer-Aided Design (3D CAD) output, without the need
6 for expensive tooling such as punches, dies or casting moulds and the assembling of multiple
7 components [4-12]. It also reduces the need for many conventional processing steps and
8 eliminates most of the constraints that hinder optimal design, creativity and ease of
9 manufacturing of complex parts. Therefore, AM is going through an exponential growth and is
10 being widely used as a novel production technology for the design and manufacturing of
11 high-performance components in the aerospace, biology, medical and energy applications [5, 7].
12 For example, complex fuel injector nozzles in aerospace technology which previously required
13 assembly of multiple parts can now be directly fabricated by AM with lightweight engineered
14 structures, resulting in significant cost savings.

15 Among several manufacturing methods, the powder-based process has attracted increasing
16 attention due to its flexibility [11, 13]. In this process, typically 10-50 μm particles are spread
17 over a work surface made of particles, which are already partially sintered/melted, by a roller or
18 blade, resulting in a particle layer with a thickness of a few particle diameters. Then a laser or
19 electron beam is shone onto it to melt the specified area. Once a cross-section is scanned, the
20 work surface is lowered and the process is repeated until the completion of the production. The
21 powder spreading process has an important effect on the quality of the powder bed for subsequent

1 sintering/melting, which in turn influences the characteristics and quality of the final product [4,
2 5]. Poor powder flow during spreading causes variations in the solid volume fraction of the
3 particle layer and roughness of its surface, leading to weak bonding between layers or formation
4 of cavities, producing inferior products with poor mechanical performance [14-16]. Lack of
5 sufficient understanding of the powder dynamics, such as the factors which influence the powder
6 flow rate through the spreader gap, hinders further refinement of this technology and introduction
7 of new materials.

8 Recently, the Discrete Element Method (DEM) has been used to describe the mechanical
9 behaviour of the powder spreading system in additive manufacturing [17-21]. Parteli and Pöschel
10 [17] and Haeri et al. [18] studied the effect of spreading speed and gap height on the bed quality
11 in the roller spreading system, and showed that high spreader translational velocity could lead to
12 low bed quality. Chen et al. [19] used spherical particles with tuned mechanical properties and
13 found that the effects of the blade spreading speed and gap height on the dynamic repose angle of
14 the heap in front of the blade were negligible. Haeri [20] explored the effect of the blade
15 geometry on the spreading performance, and found that the bed quality could be improved by
16 using a super-elliptic edge profile for the spreader. These works also showed that the powder
17 spreading process was very sensitive to powder properties (including particle size distribution,
18 interfacial surface energy, sliding friction coefficient and so on) and operation conditions
19 (including spreading speed and gap height). Nan et al. [21] characterised all the relevant physical
20 and mechanical properties of gas-atomised 316L stainless steel particles and used them in
21 numerical simulations of powder spreading by a blade. They showed that transient jamming

1 occurred in narrow spreader gaps and was manifested by the formation of empty patches over the
2 work surface. They also analysed the frequency and period of jamming and established their
3 relationships with particle properties, gap height and spread speed. The factors which have not
4 been analysed in detail so far are the powder flow rate through the spreader gap as influenced by
5 the spreader speed, as well as the shear zone in the heap in front of the blade which is responsible
6 for controlling of the powder flow rate. They are directly related to the issues during powder
7 spreading, such as the criterion for the maximum spreading throughput, and the empty patches
8 caused by the particle jamming for small spreading gaps.

9 In this work, the particle flow in the blade spreading process is simulated by Discrete
10 Element Method. The particle heap comprises gas-atomised stainless 316L steel particles. It is
11 subjected to a translational motion by a vertical blade with a gap allowing a thin particle layer to
12 be spread. The effects of the gap height and blade spreading speed on the shear zone of the
13 particle heap in front of the blade and the resulting mass flow rate through the gap are analysed.
14 This provides a benchmark for the maximum speed of the spreader, an influential factor
15 controlling the production throughput.

16 **2. Method**

17 Gas-atomised 316L stainless steel particles, provided by Sandvik Osprey Ltd, Neath, UK,
18 are modelled in this work. The characterisation of their physical and mechanical properties have
19 been done by Nan et al. [21], including the size and shape distributions, hardness and Young's
20 modulus, interfacial surface energy, coefficients of restitution and sliding friction. The particles
21 have a size distribution in the range 15-55 μm , for which the number based D_{10} , D_{50} and D_{90} are

1 20 μm , 32 μm and 45 μm , respectively. To describe the dynamics of particle flow in the spreading
 2 process, the particles are modelled as discrete entities and their motions are tracked individually
 3 by solving Newton's laws of motion [22-24], for which the EDEMTM software package provided
 4 by DEM Solutions, Edinburgh, UK, is used.

5 **2.1. Discrete Element Method**

6 According to the DEM, originally proposed by Cundall and Strack [22], the movement of an
 7 individual particle is described by the translational and rotational motions:

$$8 \quad m_i \frac{dv_i}{dt} = \sum F_{c,i} + m_i \mathbf{g} \quad (1)$$

$$9 \quad \frac{d(\mathbf{I}_i \cdot \boldsymbol{\omega}_i)}{dt} = \mathbf{R}_i \cdot \sum \mathbf{M}_{c,i} \quad (2)$$

10 where m_i , \mathbf{I}_i , \mathbf{v}_i and $\boldsymbol{\omega}_i$ are the mass, moment of inertia, translational velocity and angular velocity,
 11 respectively; $\mathbf{F}_{c,i}$ is the contact force, originating from its interaction with neighbouring particles or
 12 walls; $\mathbf{M}_{c,i}$ is the contact torque, arising from the tangential and normal contact forces; \mathbf{R}_i is the
 13 rotation matrix from the global to the local coordinate system in which the calculation of the
 14 rotation expressed by Eq. (2) is accomplished.

15 As introduced by Favier et al. [25], the non-spherical particles are described by the
 16 overlapping multi-sphere model, as shown in Fig. 1. Thus, the interactions between any two
 17 non-spherical particles can be simplified as that of spherical particles. In this work, the elastic
 18 contact force is described by Hertz-Mindlin contact model [23], and the adhesive interaction is
 19 accounted for by JKR theory [26]:

$$20 \quad F_{JKR} = 4\sqrt{\pi\gamma E^*} a^{3/2} \quad (3)$$

21 where γ is the surface energy; E^* is the equivalent Young's modulus; a is the contact radius.

1 More features and further information of the simulation method are given by Nan et al. [21] and
2 not shown here for brevity.

3 Fig. 1. Particle shapes used in DEM simulations; each size and shape class are housed in a box with coloured
4 borders, as shape varies with size; six blue boxes (15-25 μm), eight purple boxes (25-35 μm), five red boxes
5 (35-45 μm), and five green boxes (45-55 μm).

6 **2.2. Simulation Conditions**

7 The simulation system comprises a spreading blade and a base, as shown in Fig. 2, where D
8 represents the characteristic size D_{90} by number. The dimensions of the simulation domain in the
9 spreading and lateral directions are $400D$ and $10D$, respectively. The front and rear boundaries
10 (i.e. in the Y direction) are treated as periodic boundaries for particle flow. The base with the
11 same length and width as of the simulation domain is made up of clumped cylinders with axes
12 along the Y direction, where the cylinder diameter is equal to D and the distance between adjacent
13 cylinder centres is equal to $0.5D$. In this arrangement, the bulk sliding of the particles on the base
14 is mitigated by the fully-rough wall. The blade with the same width of the base has a thickness of
15 $4D$ in the spreading direction, and its height is much larger than that of the initial particle bed.

16 The initial particle bed is prepared by using the poured packing method, where
17 approximately 16,000 particles are generated. These particles have a size distribution in the range
18 15-55 μm , and are classified into four main size classes based on the equivalent-circle diameter
19 of the projected area. The number frequency for the size classes of 15-25 μm , 25-35 μm , 35-45
20 μm and 45-55 μm are 29.6%, 40.8%, 23.9% and 5.7% [21], respectively. For each size class, 5-10
21 particles are randomly selected for simulating their shapes, with a total of 24 types of shape used
22 in the simulation, as shown in Fig. 1. The physical and mechanical properties of particles, as

1 needed for numerical simulations are given in Table 1. They are characterised by special methods
2 and have been described in the previous work [21]. The integration time step is 10^{-8} s. At the start
3 of the simulation, the blade is lifted vertically to the specified position, forming a vertical gap δ
4 between the spreading blade and layering base. It is then moved along the X direction with a
5 constant velocity U , by which the particles are spread. To evaluate the effect of spreading
6 conditions on the particle flow in the spreading process, the gap δ is varied from $1.5D$ to $4.0D$, and
7 the blade speed U is varied from 0.01 m/s to 0.16 m/s.

8 Fig. 2. Schematic of particle spreading process for simulation [21].

9 Table 1. Particle properties in the simulation.

10 3. Simulation Results

11 3.1. Shear band

12 As the particle bed is subjected to the horizontal motion of the blade, a shear band is locally
13 formed around the blade. Here, the region ‘in front of the blade’ is shown in Fig. 3. Its dimensions
14 are $10D$ in the Y direction, $2.5D$ in length, in the X direction, and $6D$ in height, in the Z direction.
15 It is divided into 11 bins in the Z direction with a height equal to D , and the adjacent bins overlap
16 in height by 50%. This is done to get a smooth velocity profile. As the blade moves in the X
17 direction, only the component of particle velocity in this direction u_x is considered, and it is
18 normalised by the blade speed U .

19 Fig. 3. Illustration of the heap region ‘in front of the blade’.

20 The profile of u_x along the vertical direction is shown in Fig. 4, where the blade speed is 0.04
21 m/s. The particle velocity u_x increases with the bin centre position H and reaches a plateau when
22 H is larger than $H_l = \delta + D$. This trend suggests that the effect of blade shearing on the particles

1 mainly takes place in the zone with $H \leq \delta + D$. For a small gap height (i.e. $\delta/D=1.5$), the shear
 2 band centre position for $u_x/U=0.5$ is very close to the base, and the shear zone is not fully
 3 developed near the base, resulting in a large particle velocity at $H/D=0.5$. With the increase of the
 4 gap height, the profiles move to the right, and the velocity of particles closest to the base
 5 decreases significantly, due to further developing of the shear zone near the base. When the gap
 6 height is increased to $\delta/D=4.0$, the shear band is fully developed, resulting in a sigmoidal shape
 7 profile of particle velocity.

8 Fig. 4. Particle velocity profiles in the region ‘in front of the blade’ for different gap heights for blade speed of
 9 0.04 m/s.

10 Profiles of u_x for other blade speeds are all similar to the ones shown in Fig. 4. By rescaling
 11 of the bin centre position H in terms of $(H-h_c)/h_w$, where h_c is the shear band centre position in the
 12 vertical direction with respect to the base and h_w is a linear function of the shear band width, w ,
 13 acting as a scale factor. These profiles (i.e. totally 32 cases) all collapse onto a universal curve, as
 14 shown in Fig. 5. This curve is well fitted by the Gauss error function which is denoted by “erf”:

$$15 \quad \frac{u_x}{U} = 0.5[1 + \operatorname{erf}(\frac{H - h_c}{h_w})] \quad (4)$$

16 Thus, the profile of particle velocity could be completely described by the centre position and
 17 widths of the shear band.

18 Fig. 5. Universal curve for the particle velocity profile in the region ‘in front of the blade’.

19 The variation of the shear band centre position h_c with the blade speed is shown in Fig. 6.
 20 With the increase of blade speed, the shear band centre position moves to a lower vertical
 21 position. The shear band centre position is more sensitive to the blade speed for larger gap heights.
 22 With the increase of gap height, the shear band centre position moves to higher vertical positions,

1 which agrees well with the results shown in Fig. 4. The difference between the shear band
2 centre positions for different gap heights decreases with the blade speed. This suggests that the
3 shear band centre position is less affected by the gap height at large blade speed.

4 Here, the positions where $u_x/U=0.05$ and $u_x/U=0.95$ are regarded as the lower and upper
5 boundaries of the shear band. Thus, the shear band width, w , is calculated from the distance
6 between these two extreme positions, and is equal to $2.5h_w$, due to $0.5(1+\text{erf}(-1.25))=0.05$ and
7 $0.5(1+\text{erf}(1.25))=0.95$ in Eq. (4). The variation of the shear band width w with the blade speed
8 is shown in Fig. 7. For small blade speeds, the shear band width fluctuates with the increase of
9 gap height. For example, when the blade speed is between 0.04 m/s and 0.08 m/s, the shear band
10 width is around $3.0\text{-}3.5D$, which is also about $4.0\text{-}4.7D_V$, as $D=1.35D_V$. As the blade speed is
11 increased to 0.10 m/s and beyond, the shear band width increases almost linearly with the gap
12 height.

13 Fig. 6. Variation of the shear band centre position h_c with respect to the spread layer surface with the blade
14 speed for different gap heights.

15 Fig. 7. Variation of the shear band width w with the gap height for different blade speeds.

16 **3.2. Mass flow rate through the gap**

17 As the particle bed is sheared by the blade, particles with smaller u_x than the blade are
18 deposited onto the base through the gap. The mass flow rate is unsteady, due to the discontinuous
19 nature of particle flow in narrow openings. When the gap height is small (i.e. $\delta/D=1.5$), the
20 transient mass flow rate could even be zero, due to the particle jamming, which has been
21 discussed in detail by Nan et al. [21]. Here, the mass flow rate is time-averaged and normalised
22 by dividing it by ρWD , where ρ is particle density, W is the width of the base in the lateral

1 direction (Y direction), and D is D_{90} of particle size number distribution.

2 Variations of the mass flow rate with the blade speed are shown in Fig. 8(a). At low blade
3 speeds, the mass flow rate increases linearly with the blade speed, and its slope increases with the
4 gap height. At large blade speeds, there is a change in the trend and the mass flow rate increases
5 to an asymptotic value, which depends on the gap height. This trend suggests that the spreading
6 throughput is limited at large spreading speeds. There are therefore two flow regimes, one
7 dependent and another independent of the blade speed. It appears that the blade speed
8 corresponding to the flow regime transition is not affected by the gap height. This will be probed
9 in more detail below. The variation of mass flow rate with the gap height is shown in Fig. 8(b),
10 for which a linear relationship with the gap height is observed. The slope depends on the blade
11 speed. Thus, the following functional form is proposed for the mass flow rate:

$$12 \quad Q = \rho f_U W (\delta - \delta_c) \quad (5)$$

13 where δ_c is the critical gap height at which the mass flow rate is zero, namely the intercept on the
14 abscissa in Fig. 8(b). δ_c accounts for the boundary effects of the blade front tip, resulting in an
15 effective gap height of $\delta - \delta_c$. The dependency of the slope of the line on the blade speed is
16 expressed by f_U for the linear flow regime.

17 Fig. 8. Variation of mass flow rate with (a) blade speed and (b) gap height.

18 The variation of f_U with the blade speed is shown in Fig. 9(a). At low blade speeds U , f_U
19 increases linearly with U with a slope of about 0.55. At large blade speeds, f_U increases gradually
20 to a plateau around 0.043. Fig. 9(a) also shows there exists a critical blade speed, U_c , above which
21 the mass flow rate is almost independent of the blade speed. It is around 0.1 m/s for the particle

1 system here. The critical gap height δ_c as a function of the blade speed is shown in Fig. 9(b). Its
 2 value is around D (i.e. $1.35D_V$, where D_V is the arithmetic mean volume equivalent diameter) for
 3 the speed range 0.04-0.1 m/s, which is commonly used. In the case here, the critical gap height is
 4 caused by one side wall moving and the other being stationary, whilst the two side walls in the
 5 wedge-shaped hoppers are stationary [27-30]. Thus, the critical gap size in this work is smaller
 6 than that in hopper flow. Fig. 9 also suggests that even in the ideal case where the particles are
 7 uniformly spread onto the base without jamming, the gap height should be at least $2D$ to cover
 8 the base without any empty patches.

9 Fig. 9. Variation of (a) f_U and (b) critical gap height with blade speed.

10 The critical blade speed could also be examined by comparing the gravity inertial timescale

11 t_g and spreading inertial timescale t_s , which are defined as

$$12 \quad t_g = \sqrt{D/g} \quad (6)$$

$$13 \quad t_s = D/U \quad (7)$$

14 The gravity inertial timescale t_g is the time taken by a particle with zero initial velocity to fall a
 15 distance of $D/2$ under gravity acceleration g , whilst the spreading inertial timescale t_s is the time
 16 taken by the blade with velocity U to pass over a static particle with D . If the spreading inertial
 17 timescale is much less than the gravity inertial timescale, i.e. $t_s = t_g/k$ ($k \gg 1$), the gravity effect on
 18 the spreading process could be limited, and the particles do not have enough time to fall down to
 19 fill the dilated zone caused by the blade shearing. This could also be observed from the vertical
 20 velocity of particles in front of the blade in Fig. 3, as shown in Fig. 10. When the blade speed is
 21 0.1 m/s or greater, the falling velocity of particles (i.e. $-u_z$) does not show any further increase

1 with the increase of U , indicating that no more additional particles could move to the dilated zone
2 as the blade speed is increased. Therefore, by comparing t_s and t_g , a critical blade speed could
3 be defined as:

$$4 \quad U_c = k\sqrt{gD} \quad (8)$$

5 where k is the ratio of the two timescales ($\gg 1$). The variation of the critical blade speed with k is
6 shown in Table 2. In this work, $k=5$ gives the same critical blade speed (i.e. 0.1 m/s) as given in
7 the description of Figs. 8 and 9. Therefore, the critical blade speed is well described by Eq. (8).

8 Fig. 10. Profiles of u_z in the heap in front of the blade for different blade speeds for the gap height of $\delta/D=3.0$.

9 Table 2. Variation of critical blade speed with k .

10 4. Conclusions

11 The particle spreading process in additive manufacturing has been analysed by DEM
12 simulations, using realistic physical and mechanical properties of particles as measured for single
13 particles in the previous work. The effect of the spreading process on the particle flow has been
14 analysed in terms of the shear band and mass flow rate through the gap height. The main results
15 from the present study are summarised as follows:

16 1) The velocity profiles of particles in the heap in front of the blade follow a universal curve
17 given by the Gauss error function. With the increase of blade speed or the decrease of the gap
18 height, the shear band centre moves to lower vertical positions.

19 2) The mass flow rate through the gap increases linearly with the gap height. There is a
20 critical size of about D below which there is no flow. The dependence of the mass flow rate on
21 the blade speed is more complex. There are two different flow regimes. The mass flow rate is
22 initially linear but approaches an asymptotic value at large blade speeds. The transition point

1 from linear to the asymptotic trend is independent of the gap height. The critical blade spreading
2 speed, above which the mass flow rate is independent on the blade spreading speed, is 0.1 m/s for
3 the system studied here.

4 3) The critical blade spreading speed could be examined by comparing the gravity inertial
5 timescale and spreading inertial timescale, and it is about $5(gD)^{0.5}$.

6 **Acknowledgements**

7 The authors are thankful to DEM Solutions, Edinburgh, UK, for providing a special license
8 for the EDEM software for use in this work.

9 **Reference**

- 10 [1] S. Antoniw, N. McCarthy, E. Pacey, B. Parkin, P. Shelton, Additive Manufacturing: Opportunities and Constraints,
11 Royal Academy of Engineering, 2013, pp. 1-21.
- 12 [2] B. Berman, 3-D printing: The new industrial revolution, *Business Horizons*, 55 (2012) 155-162.
- 13 [3] U.M. Dilberoglu, B. Gharehpapagh, U. Yaman, M. Dolen, The Role of Additive Manufacturing in the Era of
14 Industry 4.0, *Procedia Manufacturing*, 11 (2017) 545-554.
- 15 [4] T. DebRoy, H.L. Wei, J.S. Zuback, T. Mukherjee, J.W. Elmer, J.O. Milewski, A.M. Beese, A. Wilson-Heid, A. De,
16 W. Zhang, Additive manufacturing of metallic components – Process, structure and properties, *Progress in*
17 *Materials Science*, 92 (2018) 112-224.
- 18 [5] I. Gibson, D. Rosen, B. Stucker, Additive manufacturing technologies, 3D printing, rapid prototyping, and direct
19 digital manufacturing, Springer, New York, 2015.
- 20 [6] W.E. Frazier, Metal Additive Manufacturing: A Review, *Journal of Materials Engineering and Performance*, 23
21 (2014) 1917-1928.
- 22 [7] N. Guo, M.C. Leu, Additive manufacturing: technology, applications and research needs, *Frontiers of Mechanical*
23 *Engineering*, 8 (2013) 215-243.
- 24 [8] T.D. Ngo, A. Kashani, G. Imbalzano, K.T.Q. Nguyen, D. Hui, Additive manufacturing (3D printing): A review of
25 materials, methods, applications and challenges, *Composites Part B: Engineering*, 143 (2018) 172-196.
- 26 [9] S.M. Thompson, L. Bian, N. Shamsaei, A. Yadollahi, An overview of Direct Laser Deposition for additive
27 manufacturing; Part I: Transport phenomena, modeling and diagnostics, *Additive Manufacturing*, 8 (2015) 36-62.
- 28 [10] N. Shamsaei, A. Yadollahi, L. Bian, S.M. Thompson, An overview of Direct Laser Deposition for additive
29 manufacturing; Part II: Mechanical behavior, process parameter optimization and control, *Additive*
30 *Manufacturing*, 8 (2015) 12-35.
- 31 [11] S. Singh, S. Ramakrishna, R. Singh, Material issues in additive manufacturing: A review, *Journal of*
32 *Manufacturing Processes*, 25 (2017) 185-200.
- 33 [12] S.F. Shirazi, S. Gharekhani, M. Mehrali, H. Yarmand, H.S. Metselaar, N. Adib Kadri, N.A. Osman, A review on

- 1 powder-based additive manufacturing for tissue engineering: selective laser sintering and inkjet 3D printing,
2 Science and Technology of Advanced Materials, 16 (2015) 033502.
- 3 [13] D.D. Gu, W. Meiners, K. Wissenbach, R. Poprawe, Laser additive manufacturing of metallic components:
4 materials, processes and mechanisms, International Materials Reviews, 57 (2013) 133-164.
- 5 [14] A. Townsend, N. Senin, L. Blunt, R.K. Leach, J.S. Taylor, Surface texture metrology for metal additive
6 manufacturing: a review, Precision Engineering, 46 (2016) 34-47.
- 7 [15] S.A. Khairallah, A.T. Anderson, A. Rubenchik, W.E. King, Laser powder-bed fusion additive manufacturing:
8 Physics of complex melt flow and formation mechanisms of pores, spatter, and denudation zones, Acta Materialia,
9 108 (2016) 36-45.
- 10 [16] P. Bidare, R.R.J. Maier, R.J. Beck, J.D. Shephard, A.J. Moore, An open-architecture metal powder bed fusion
11 system for in-situ process measurements, Additive Manufacturing, 16 (2017) 177-185.
- 12 [17] E.J.R. Parteli, T. Pöschel, Particle-based simulation of powder application in additive manufacturing, Powder
13 Technology, 288 (2016) 96-102.
- 14 [18] S. Haeri, Y. Wang, O. Ghita, J. Sun, Discrete element simulation and experimental study of powder spreading
15 process in additive manufacturing, Powder Technology, 306 (2016) 45-54.
- 16 [19] H. Chen, Q. Wei, S. Wen, Z. Li, Y. Shi, Flow behavior of powder particles in layering process of selective laser
17 melting: Numerical modeling and experimental verification based on discrete element method, International
18 Journal of Machine Tools and Manufacture, 123 (2017) 146-159.
- 19 [20] S. Haeri, Optimisation of blade type spreaders for powder bed preparation in Additive Manufacturing using DEM
20 simulations, Powder Technology, 321 (2017) 94-104.
- 21 [21] W. Nan, M. Pasha, T. Bonakdar, A. Lopez, U. Zafar, S. Nadimi, M. Ghadiri, Jamming during particle spreading in
22 additive manufacturing, Powder Technology, 338 (2018) 253-262.
- 23 [22] P.A. Cundall, O.D.L. Strack, A discrete numerical model for granular assemblies, Géotechnique, 29 (1979) 47-65.
- 24 [23] C. Thornton, Granular Dynamics, Contact Mechanics and Particle System Simulations, Springer, New York,
25 2015.
- 26 [24] W. Nan, M. Ghadiri, Y. Wang, Analysis of powder rheometry of FT4: Effect of particle shape, Chemical
27 Engineering Science, 173 (2017) 374-383.
- 28 [25] J.F. Favier, M.H. Abbaspour-Fard, M. Kremmer, A.O. Raji, Shape representation of axi-symmetrical,
29 non-spherical particles in discrete element simulation using multi-element model particles, Engineering
30 Computations, 16 (1999) 467-480
- 31 [26] K. Johnson, K. Kendall, A. Roberts, Surface energy and the contact of elastic solids, Proceedings of the Royal
32 Society of London. A. Mathematical and Physical Sciences, 324 (1971) 301-313.
- 33 [27] K. To, P.Y. Lai, H.K. Pak, Jamming of granular flow in a two-dimensional hopper, Phys Rev Lett, 86 (2001) 71-74.
- 34 [28] R.P. Behringer, Dynamics and rheology of cohesive and deformable granular materials, Jamming and Flow in a
35 Hopper, IFPRI Report, 2007, pp. 1-3.
- 36 [29] D. Schulze, Powders and Bulk Solids Behavior, Characterization, Storage and Flow, Verlag Berlin Heidelberg,
37 Springer, 2007.
- 38 [30] N.R. M, Statics and Kinematics of Granular Materials, Cambridge University Press, Cambridge, 2005.
- 39

1

Table 1. Particle properties in the simulation.

Parameters	Value
Particle diameter, D (mm)	0.045
Particle density, ρ (kg/m ³)	7980
Young's modulus, E (GPa)	2.1
Poisson ratio, ν	0.3
Friction coefficient, μ	0.5
Restitution coefficient, e	0.64
Surface energy, γ (mJ/m ²)	1.4

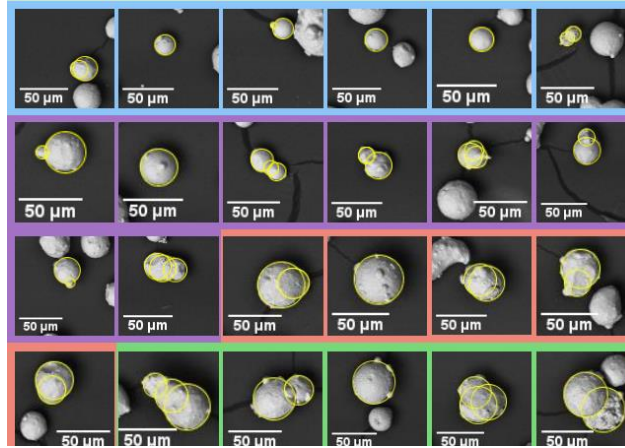
2

1

Table 2. Variation of critical blade speed with k .

k	3	4	5	6	7
U_c (m/s)	0.063	0.084	0.105	0.126	0.147

2



1
2 Fig. 1. Particle shapes used in DEM simulations; each size and shape class are housed in a box with coloured
3 borders, as shape varies with size; six blue boxes (15-25 μm), eight purple boxes (25-35 μm), five red boxes
4 (35-45 μm), and five green boxes (45-55 μm).

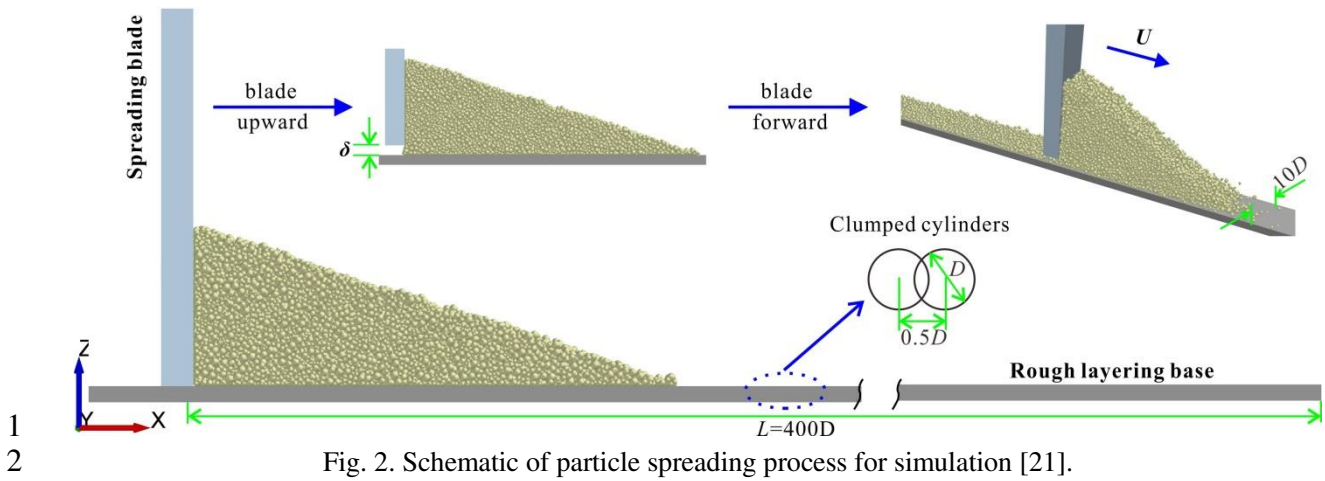
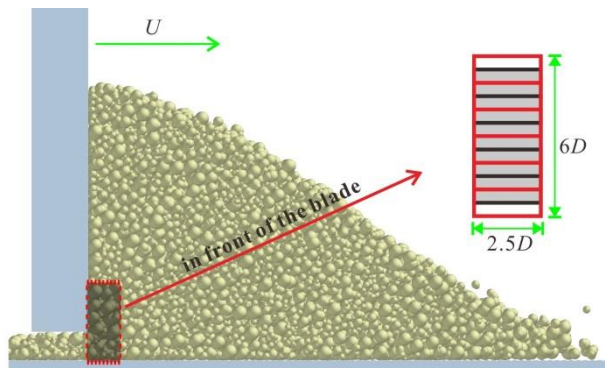
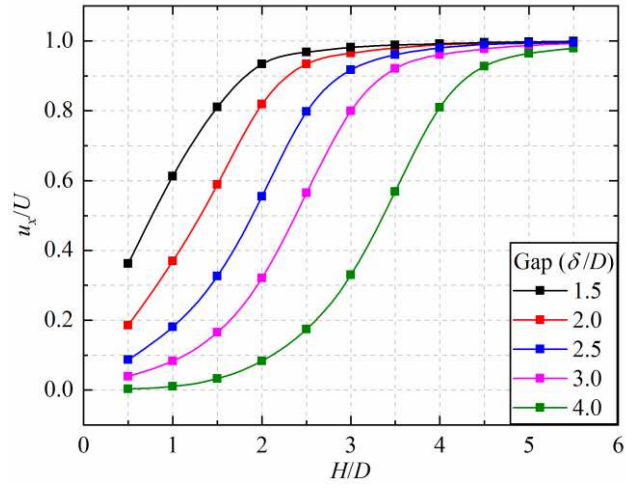


Fig. 2. Schematic of particle spreading process for simulation [21].



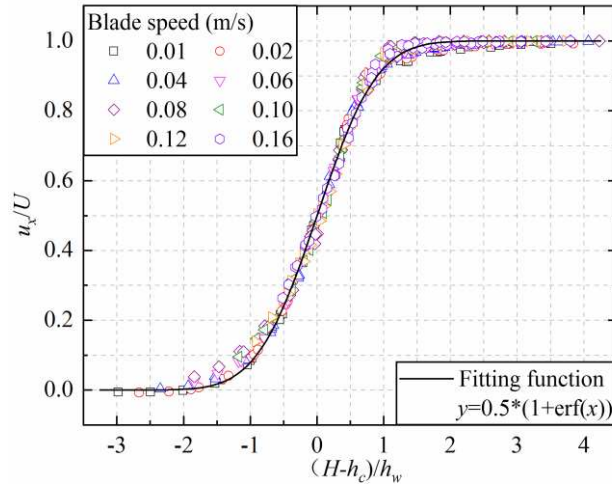
1
2

Fig. 3. Illustration of the heap region 'in front of the blade'.

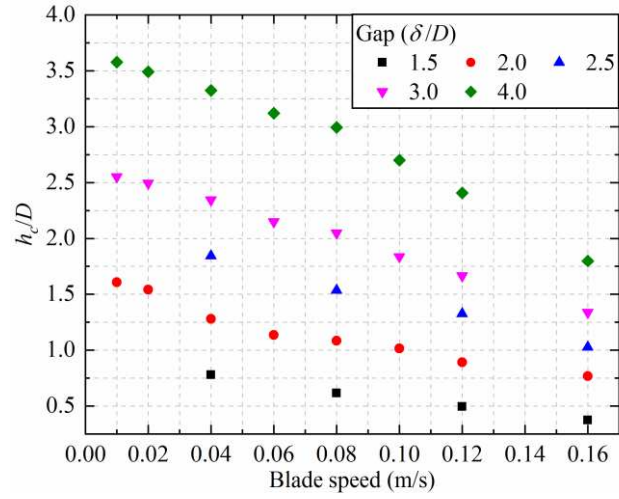


1

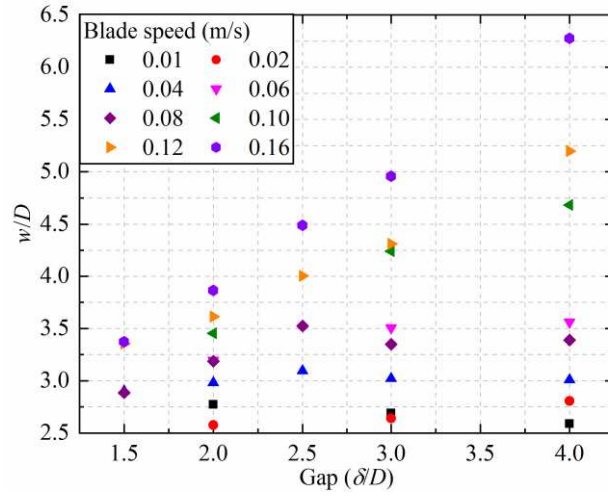
2 Fig. 4. Particle velocity profiles in the region ‘in front of the blade’ for different gap heights for blade speed of
 3 0.04 m/s.



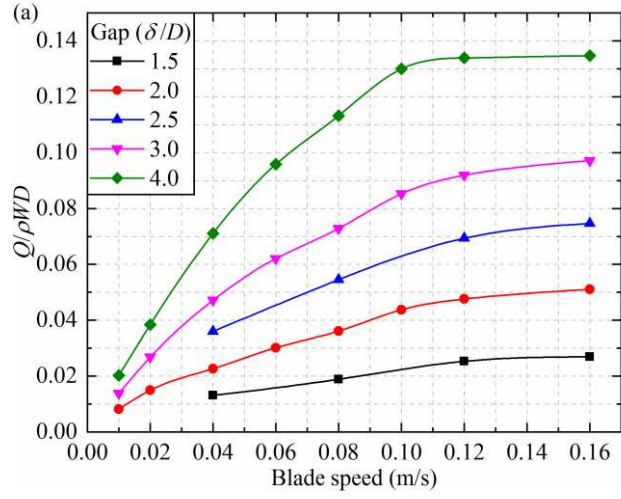
1
 2 Fig. 5. Universal curve for the particle velocity profile in the region ‘in front of the blade’.



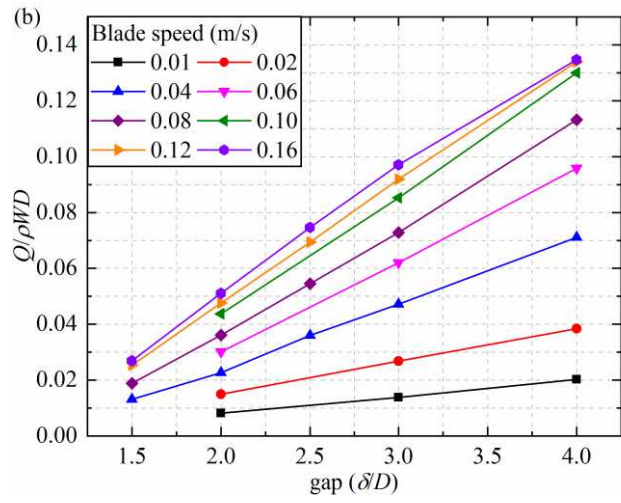
1
 2 Fig. 6. Variation of the shear band centre position h_c with respect to the spread layer surface with the blade
 3 speed for different gap heights.



1
2 Fig. 7. Variation of the shear band width w with the gap height for different blade speeds.



1

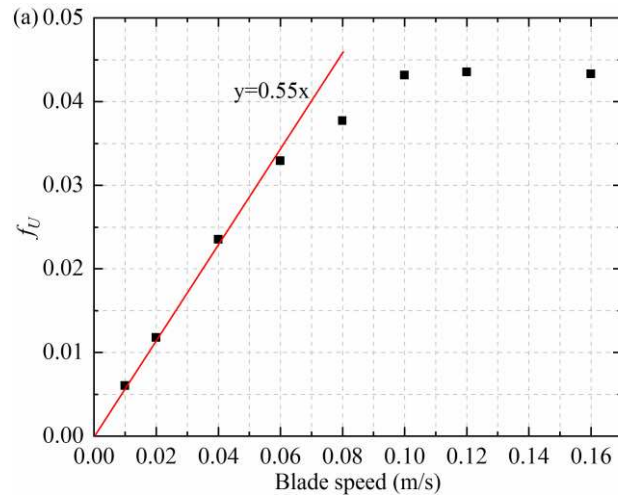


2

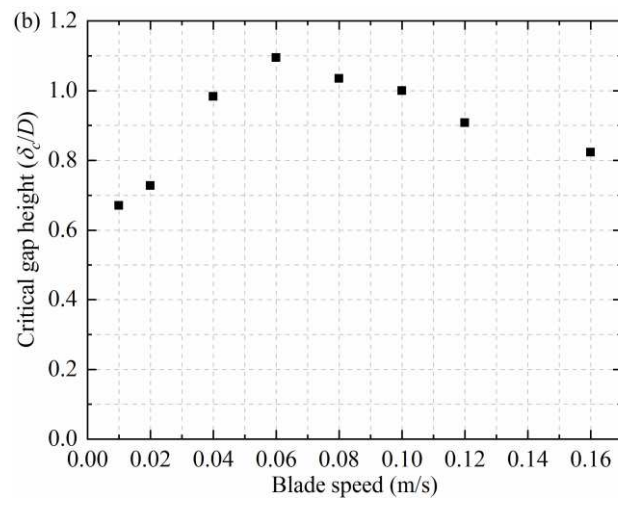
3

Fig. 8. Variation of mass flow rate with (a) blade speed and (b) gap height.

1

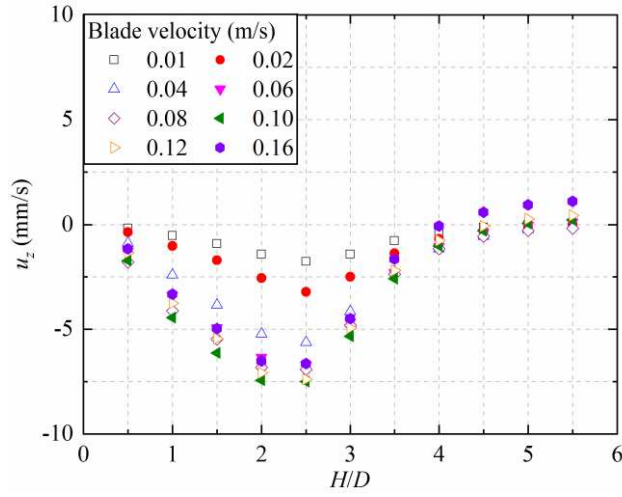


2



3

Fig. 9. Variation of (a) f_v and (b) critical gap height with blade speed.



1
 2 Fig. 10. Profiles of u_z in the heap in front of the blade for different blade speeds for the gap height of $\delta/D=3.0$.
 3